Molecular Neurobiology (2021) 58:3641–3652
https://doi.org/10.1007/s12035-021-02371-4

Evaluation of a Low-Toxicity PARP Inhibitor as a Neuroprotective Agent for Parkinson's Disease

Laura N. Puentes[1] · Zsofia Lengyel-Zhand[2] · Sean W. Reilly[2] · Robert H. Mach[2]

Received: 11 December 2020 / Accepted: 22 March 2021 / Published online: 31 March 2021

Abstract

Repurposing PARP-1 inhibitors (PARPi) for non-oncological applications offers an attractive therapeutic strategy for pathological conditions characterized by PARP-1 hyperactivity. In the context of Parkinson's disease (PD), PARP-1 hyperactivity has been linked to neuronal death and disease progression. From a therapy perspective, the evaluation of PARPi as neuroprotective agents may offer a new therapeutic alternative for neurodegenerative disorders. An ideal PARPi needs to inhibit PARP-1 hyperactivity while also limiting downstream DNA damage and cellular toxicity—an effect that is attractive in cancer but far from ideal in neurological disease applications. Consequently, in this study, we set out to evaluate the neuroprotective properties of a previously reported low-toxicity PARPi (**10e**) using in vitro neuronal models of PD. **10e** is a structural analogue of FDA-approved PARPi olaparib, with high PARP-1 affinity and selectivity. Our studies revealed that **10e** protects neuronal cells from oxidative stress and DNA damage. In addition, **10e** exhibits neuroprotective properties against α-synuclein pre-formed fibrils (αSyn PFF) mediated effects, including reduction in the levels of phosphorylated αSyn and protection against abnormal changes in NAD^+ levels. Our in vitro studies with **10e** provide support for repurposing high-affinity and low-toxicity PARPi for neurological applications and lay the groundwork for long-term therapeutic studies in animal models of PD.

Keywords Poly(ADP-ribose) polymerase-1 · PARP inhibitor · Parkinson's disease · Alpha-synuclein · Pre-formed fibrils · Poly(ADP-ribose) · Nicotinamide adenine dinucleotide

Introduction

Poly(ADP-ribose) polymerase-1 (PARP-1), a multifunctional nuclear enzyme, has been implicated in various diseases such as human malignancies, myocardial infarction, stroke, and neurodegenerative disorders [1–4]. Under physiological settings, PARP-1 is involved in DNA repair—including repair of double-strand breaks and single-strand breaks—in the modification of chromatin structure and in transcription regulation [5, 6]. Upon DNA damage, the protein binds to the damaged site, which stimulates its catalytic activity through an allosteric activation, leading to increased utilization of substrate nicotinamide adenine dinucleotide (NAD^+) to synthesize negatively charged poly(ADP-ribose) (PAR) chains on itself (automodification) or other target proteins (PARylation) [7]. Generation of PAR signals the presence of DNA damage, and components of the DNA repair machinery are recruited to the site, while PARP-1 releases the DNA to allow DNA repair. In pathological conditions involving inflammation and extensive DNA damage, PARP-1 hyperactivation leads to parthanatos, a type of cell death that is mediated by accumulation of excess PAR, depletion of cellular energy sources, and release of apoptosis-inducing factor (AIF) from the mitochondria [8].

PARP-1 hyperactivity has been linked to various neurodegenerative disorders, including amyotrophic lateral sclerosis (ALS) [9], Alzheimer's disease (AD) [10], Parkinson's disease (PD) [11], and Huntington disease (HD) [12]. In the context of PD, accumulation of phosphorylated and high molecular weight (HMW) forms of the protein alpha-synuclein (αSyn) have been directly implicated in PD pathogenesis and progression [13]. Furthermore, studies have shown that exogenous administration of αSyn pre-formed fibrils (PFFs) in neurons increase nitric oxide production leading to extensive

✉ Robert H. Mach
rmach@pennmedicine.upenn.edu

[1] Department of Systems Pharmacology and Translational Therapeutics, University of Pennsylvania, Philadelphia, PA 19104, USA

[2] Department of Radiology, Perelman School of Medicine, University of Pennsylvania, Philadelphia, PA 19104, USA

DNA damage, PARP-1 hyperactivation, and excess accumulation of PAR polymer—the latter has been implicated in promoting αSyn aggregation and driving αSyn-mediated toxicity [11] and NAD^+ depletion [8]. Studies have also shown that PARP-1 inhibition confers neuroprotective effects [14–16]. Therefore, targeting PARP-1 may offer an attractive therapeutic intervention for the treatment of neurodegenerative diseases such as PD.

Currently a number of different PARP-1 inhibitors (PARPi) have been approved by the FDA for BRCA1/2-mutated cancer therapies, including olaparib, rucaparib, niraparib, and talazoparib [17–20]. These clinical PARPi bind to the catalytic center of the enzyme, blocking the binding of NAD^+ and PAR production. In addition, these class of inhibitors modulate PARP-1 allostery and trap the enzyme onto chromatin (PARP-1 trapping). Upon inhibition of PARP-1, cell death is induced by increasing the number of double-strand DNA breaks. Additionally, recent findings indicate that trapping potency of PARPi is directly linked to cytotoxicity [21].

Given the apparent involvement of PARP-1 in neurodegenerative diseases, repurposing PARPi for non-oncological purposes might provide a facilitated route for a novel therapy for patients with PD. Repurposing PARPi is an attractive new strategy in drug research since it could offer a low cost and accelerated development of a new treatment. Here, we set out to investigate the neuroprotective effects of a recently reported PARP-1 inhibitor [22]. The compound is part of a series of olaparib analogues where the piperazine core was replaced with a diazaspiro system with the aim of lowering toxicity. The best-in-class compound, **10e**, displayed selectivity and high-affinity for PARP-1 (IC_{50} 12 nM) and reduced ability to cause DNA damage. Since non-oncological diseases would benefit from PARP-1 inhibition, but not cell death, the low toxicity of **10e** makes it an appealing candidate for neurological applications. In this paper, we further investigate the PARP-1 inhibitory properties and neuroprotective properties of **10e** using in vitro neuronal cell culture. We show that **10e** not only protects neuronal cells from DNA damage and oxidative stress but also reduces the levels of phosphorylated αSyn and displays pronounced neuroprotective effects when compared to its toxic analogue, olaparib.

Results

10e Is Less Cytotoxic than Olaparib, Veliparib, and PJ-34

To evaluate the therapeutic potential of **10e**, we treated human neuroblastoma cells (SH-SY5Y-WT) with a single dose of PARPi (10μM) for 7 days and quantified cell viability using a luminescence-based assay (Fig. 1a). The aim of this experiment was to compare the cytotoxic properties of **10e** against olaparib and a number of olaparib analogues originally identified by our group [22] (Table 1). To further expand on the scope of this experiment, we included veliparib and PJ-34 as well, since both of these PARPi have been extensively studied in non-oncological disease settings in part due to their lower toxicity profiles [11, 23]. Veliparib is a clinically relevant PARPi that is currently under evaluation in a number of combination therapy clinical trials [24], while PJ-34 is a PARPi that was previously evaluated as a cardioprotective agent in pre-clinical models of cardiotoxicity [25]. In addition to single-dose viability assays (Fig. 1a), we also established a full dose-response curve for olaparib, veliparib, and **10e** using the human neuroblastoma cell line IMR-5 (Fig. 1b). IMR-5 is a neuronal line that is highly sensitive to genotoxic stress [26]; therefore, the use of this cell line serves as an adequate model for the evaluation of differential cytotoxicity measurements between **10e**, olaparib, and veliparib.

10e Has Lower PARP-2 Trapping Potency Compared to PJ-34

Our group previously evaluated off-target interactions for **10e** and olaparib [22] and found **10e** to have better PARP-1 selectivity than olaparib. In this present study, we decided to characterize the differences in PARP-2 trapping potencies (i.e., stabilization of PARP-2/DNA complexes) for the different PARPi. To do this, we used a microscopy-based PARP-2 trapping assay previously described by Michelena and colleagues [27] and treated SH-SY5Y-WT cells with a 10 μM dose of PARPi for 24 h, followed by immunostaining for chromatin-bound PARP-2 using a PARP-2-specific antibody. Individual cell nuclei were then counted, and PARP-2-integrated intensities for each nuclei were then measured using CellProfiler 3.5.1 software. Mean values were plotted in a bar graph to compare the PARP-2-integrated intensities for all PARPi treatments (Fig. 1c). Based on the results from the fluorescence-based PARP-2 trapping assay, we noted that the PARP-2 signal intensity for the cell samples treated with PJ-34 was the highest among all the PARPi treatments. This was not surprising given that PJ-34 has higher affinity for PARP-2 compared to PARP-1 [23]. Notably, **10e** showed decreased signal intensity compared to PJ-34 and comparable signal intensity compared to veliparib and olaparib. The olaparib analogues **10a**, **10b**, **12a**, **14a**, and **15a** all displayed higher PARP-2 trapping potencies, indicating possible "off-target" effects and thus limiting their utility as PARP-1-selective inhibitors (Fig. 1c). Next, we aimed to confirm the specificity of **10e** for PARP-1. To do this, we edited IMR-5 cells using CRISPR/Cas9 [28] to generate a PARP-1/KO neuronal line (IMR-5 PARP-1/KO). The edited cells were then treated with varying doses of **10e** to generate a dose-response curve (Fig. 1d). IMR-5-Cas9 cells expressing WT PARP-1

Table 1 Chemical structure of FDA-approved olaparib and olaparib analogues and their PARP-1 IC_{50} values. Dose-response curves were produced to calculate 50% maximum inhibition values (IC_{50}) [22]. IC_{50} values represent inhibition of PARP-1 enzymatic activity

Name	Structure		IC_{50} (nM)
olaparib	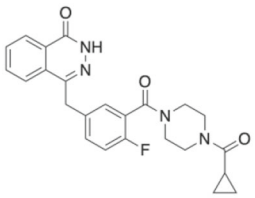	-	6.0
10a	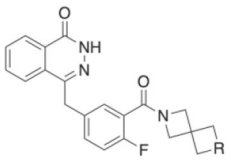	R = CH_2	39.5
10b		R = O	24.9
10e		R = 	12.6
12a	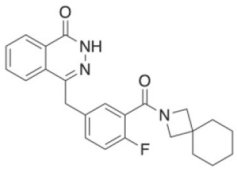	-	65.4
14a	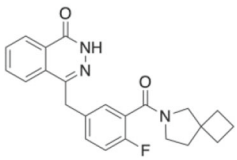	-	32.4
15a	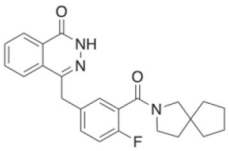	-	51.4
17a	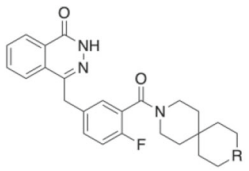	R = CH_2	57.1
17d		R = 	44.3

(IMR-5 PARP-1/WT) were used as isogenic controls for these experiments. Based on our results, we noted a rightward shift in the dose-response curve for the IMR-5 PARP-1 K/O cells compared to the IMR-5 PARP-1/WT line, indicating that upon loss of PARP-1, the pharmacological potency of **10e** gets notably diminished. Finally, since very high doses (>300 μM) of **10e** were needed to generate a shouldered dose-response curve with this compound, it can be deduced that any cell death effects in the PARP-1 K/O line were likely due to off-target activity stemming from non-PARP-1-mediated effects.

10e Protects Neuronal Cells Against DNA Damage and Oxidative Stress-Induced Cell Death

To evaluate if **10e** protects SH-SY5Y-WT neuronal cells from DNA damage-induced cell death and whether these protective effects are equipotent to olaparib and veliparib, cells were pretreated with a 10 μM dose of either olaparib, veliparib, or **10e** and then treated with the DNA-alkylating agent methyl methanesulfonate (MMS) for 4 h. Following treatment, a luminescence-based assay was used to measure cell viability. As a positive control, we included a "no PARPi" condition

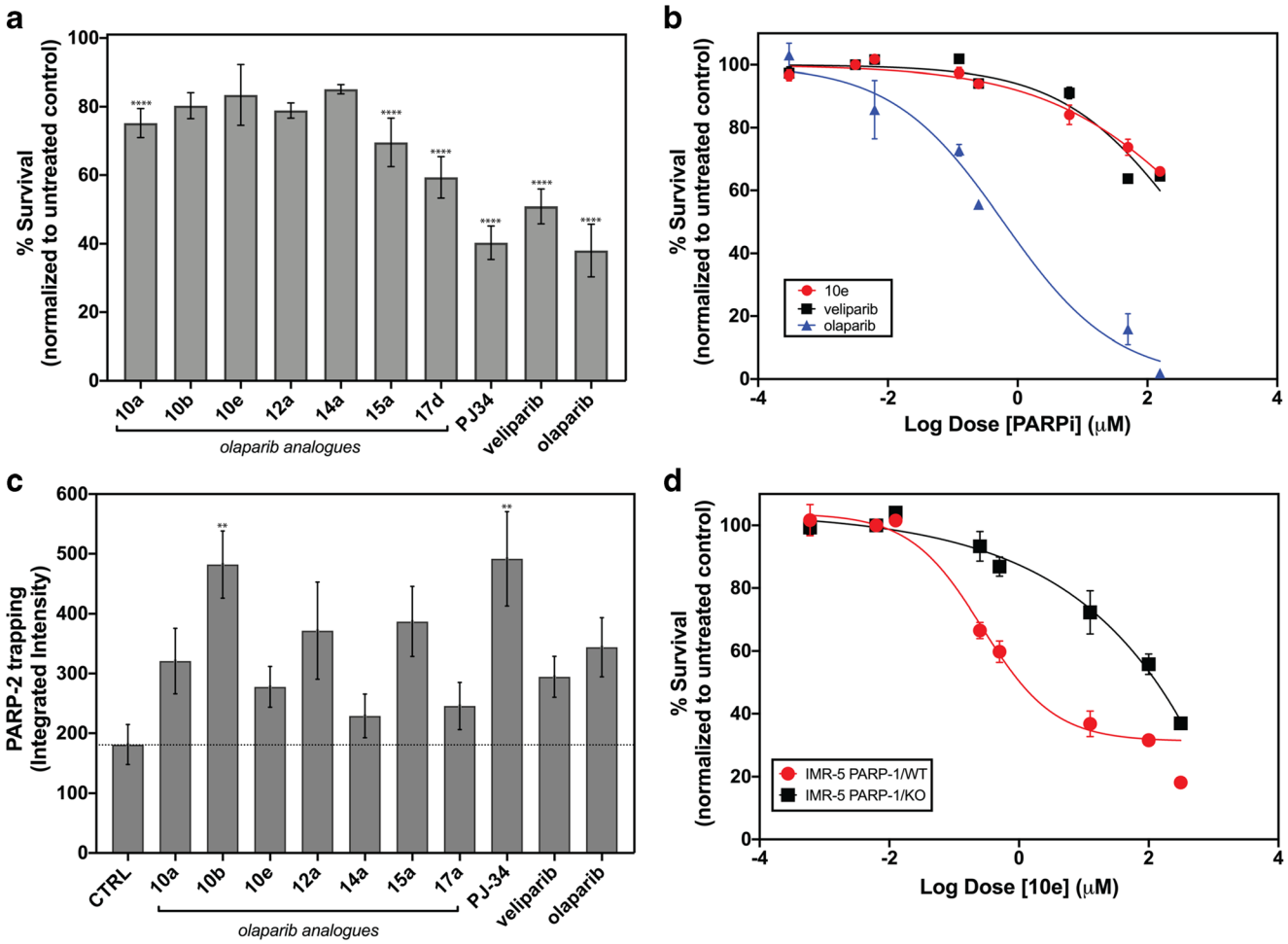

Fig. 1 (**a**) In vitro toxicity assay in SH-SY5Y-WT cells following treatment with a 10 μM dose of PARPi for 7 days. Bars represent means ± SEM. (n =3). ****$P < 0.0001$. (**b**) Dose-response curve comparing the cytotoxic effects of **10e** (*red circles*), veliparib (*black squares*), and olaparib (*blue triangles*) in IMR-5 neuroblastoma cells. Symbols represent means ± SEM (n =3). (**c**) PARP-2 trapping assay to assess PARP-2 selectivity of **10e**, olaparib analogues (**10a**, **10b**, **10e**, **12a**, **14a**, **15a**, **17a**), veliparib, olaparib, and PJ-34. Bars represent means ± SEM (n=3). **$P < 0.001$. (d) A luminescence-based cell viability assay was used to measure and compare the pharmacological effects of **10e** in both PARP-1/WT vs. PARP-1/KO IMR-5 cells. Symbols represent means ± SEM (n =3)

whereby cells were treated with MMS only. Output values were then normalized to the no-treatment control and plotted as percent (%) survival (Fig. 2a). Similarly, to assess if **10e** protects neuronal cells from oxidative stress, cells were pre-treated with **10e**, followed by treatment with H_2O_2 for 30 min. The neuroprotective properties of **10e** were then evaluated against olaparib and veliparib in order to assess if **10e** exerts comparable therapeutic effects to these PARPi (Fig. 2b).

10e Is Unable to Induce DNA Damage at Concentrations as High as 10 μM

Previously [22], we characterized the DNA damaging properties of olaparib and **10e** via immunofluorescence (IF) staining of γH2AX, a known biomarker for DNA double-strand breaks [29]. From these studies [22], we reported that olaparib induces DNA damage in a dose-dependent manner and that **10e** fails to induce DNA damage even at concentrations as high as 10 μM. Herein, we performed a similar experiment, whereby cells were treated with a 10 μM dose of either olaparib, veliparib, or **10e** for 24 h and then processed for anti-RAD51 IF in order to detect nuclear RAD51 foci formation, as a proxy marker of DNA damage [30] (Fig. 2 c and d).

10e Is Less Potent than Olaparib at Trapping PARP-1

All FDA-approved PARPi (olaparib, rucaparib, niraparib, and talazoparib) bind the NAD^+ binding pocket of PARP-1 and induce structural changes to the enzyme that result in PARP-1 becoming "trapped" at sites of DNA damage [21]. This trapping effect generates lesions in DNA that become toxic over time. To assess the trapping potency of **10e** (Fig. 3 a and b), we followed a biochemical PARP-1 trapping assay whereby cells were first pre-treated with PARPi, followed by treatment

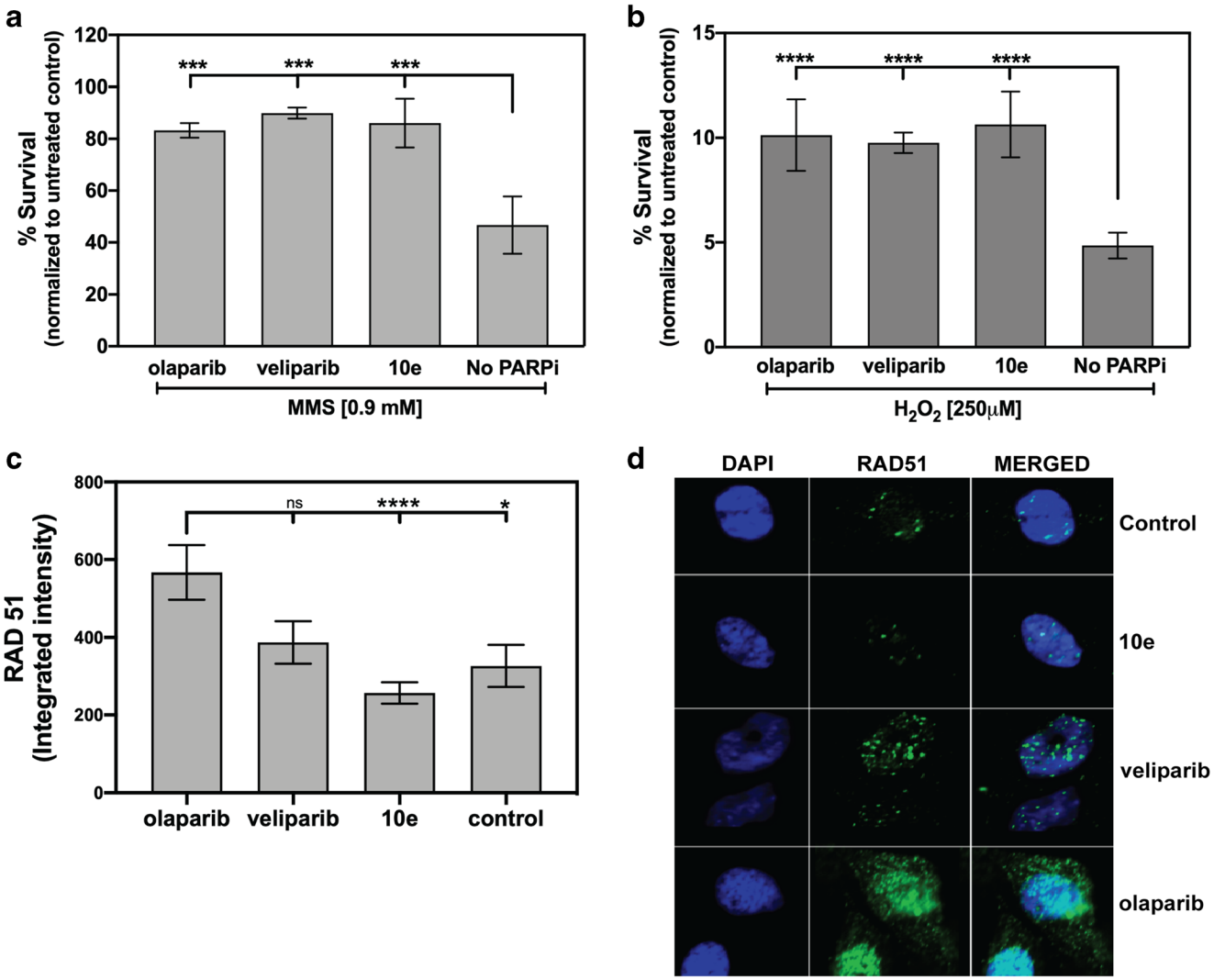

Fig. 2 (**a**) Percent survival measurements following a 4-h treatment with MMS in the presence or absence of PARPi (olaparib, veliparib, or **10e**). Bars represent means ± SEM (n =3). ***$P < 0.001$. (**b**) Percent survival measurements following a 30-min treatment with H_2O_2 in the presence or absence of PARPi (olaparib, veliparib, or **10e**). Bars represent means ± SEM (n =3). ****$P < 0.0001$. (**c**) Nuclear RAD51 foci integrated signal intensity for olaparib, veliparib, or **10e**-treated samples. Bars represent means ± SEM (n =3). *$P < 0.01$, ****$P < 0.0001$. (**d**) Representative ROIs of RAD51 staining (green) and DAPI (blue)

with MMS to induce DNA damage [31]. Following treatment, the cells were washed, and lysates were collected and separated into subcellular fractions using a commercially available kit. The chromatin-bound fractions were then immunoblotted for PARP-1 (Fig. 3b) and evaluated against the following two controls: no treatment and PARPi treatment only. Olaparib-only and olaparib + MMS conditions were also included in this assay to compare the trapping potency of **10e** against olaparib (Fig. 3 a and b). We observed significant trapping differences between **10e** and olaparib in the presence of MMS (Fig. 3a) and a modest increase in PARP-1 trapping in the olaparib-only treated samples (Fig. 3a). To further validate our results, we also performed a microscopy-based PARP-1 trapping assay in order to compare the PARP-1 trapping potencies of **10e**, olaparib, and veliparib in the absence of MMS treatment (Fig. 3 c and d). Similar to the PARP-2 trapping assay, cells were treated with 10 μM PARPi for 24 h and then immunostained for PARP-1 using a PARP-1-specific antibody. Results from these experiments suggest that even at a dose (10 μM) where **10e** elicits 100% PARP-1 enzyme inhibition [22], the PARP-1 trapping potency of **10e** is notably lower compared to olaparib. Interestingly, **10e** displayed a similar PARP-1 trapping potency to veliparib in the microscopy-based assay (Fig. 3 c and d), suggesting that **10e**-mediated PARP-1 trapping might be closer to veliparib than olaparib.

10e Exerts Neuroprotective Effects in a Neuronal Model of Alpha-Synuclein Aggregation

To assess the therapeutic potential of **10e** in a PD-like model, we employed the use of a human neuroblastoma cell line (SH-

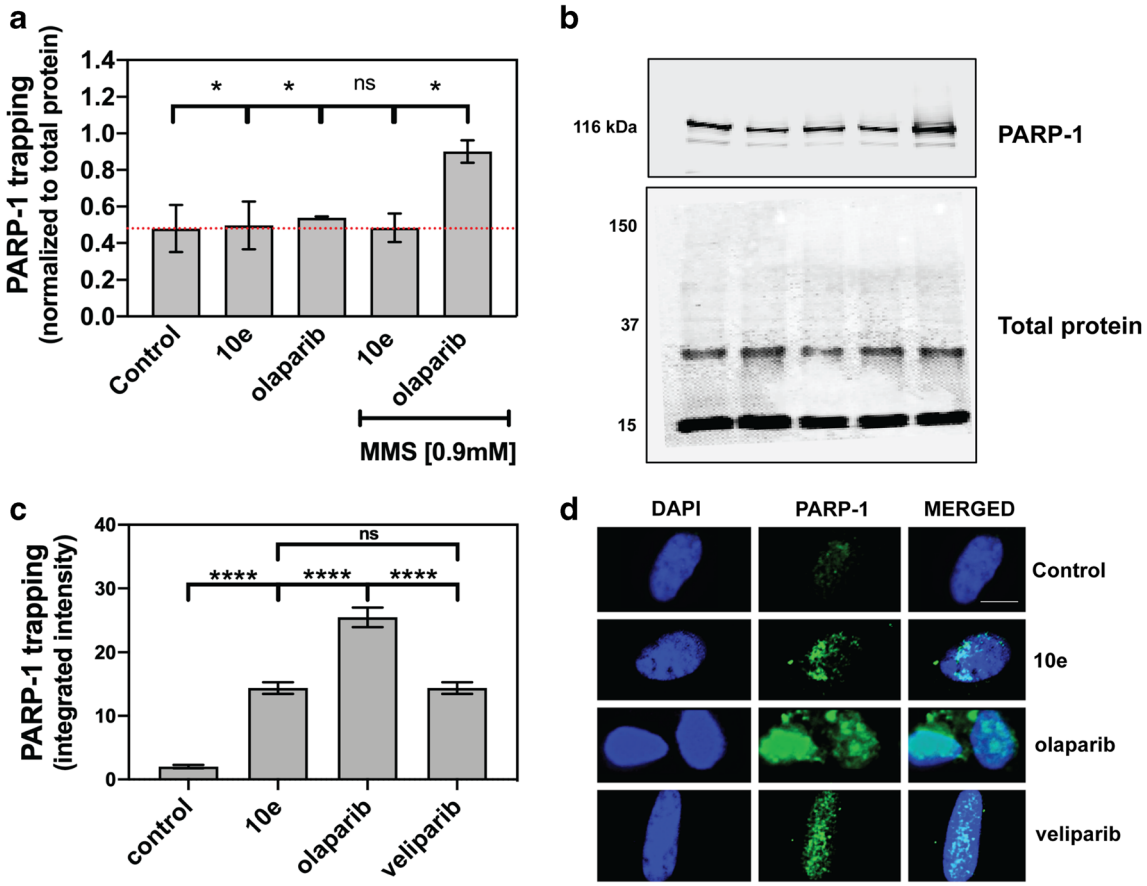

Fig. 3 (**a**) Biochemical PARP-1 trapping assay to assess trapping potency between **10e** and olaparib in the absence or presence of MMS treatment. Bars represent means ± SEM (n =3). *$P < 0.01$. (**b**) *(From left-to-right)* untreated control, **10e**-only treatment, olaparib-only treatment, **10e** + MMS, and olaparib + MMS. Samples were treated for 4 h. Columns represent PARP-1 intensity values normalized by total protein intensity per lane. REVERT 700 total protein stain was used to stain all proteins. Bars represent means ± SEM (n =3). (**c**) Microscopy-based PARP-1 trapping assay. PARPi treatment was increased to 24 h, and PARP-1 signal intensity was measured for each treatment condition. Bars represent mean integrated intensity ± SEM (n =3). ****$P < 0.0001$. (**d**) Representative ROIs of PARP-1 staining (green) and DAPI (blue)

SY5Y-WT) stably transduced to overexpress WT αSyn (SH-SY5Y-αSyn). Since phosphorylated/high molecular weight (HMW) forms of αSyn (> 25 kDa) drive Parkinson's disease (PD) progression and neurotoxicity [11] (Fig. 4a), we induced the formation of phosphorylated/HMW αSyn aggregates by treating SH-SY5Y-αSyn cells with αSyn PFFs (500 nM) for 48 h. We then measured αSyn PFF-induced PARP-1 hyperactivation (i.e., excess PAR polymer production) (Fig. 4b) and αSyn aggregate formation (Fig. 4c) and then tested whether pre-treatment with **10e** (10 μM) 2 h before αSyn PFF (500 nM) treatment (αSyn PFFs + **10e**) had any effect on PFF-induced PARP-1 hyperactivation (Fig. 4b) and/or HMW αSyn aggregate formation (Fig. 4c). Furthermore, since PARP-1 hyperactivation leads to NAD^+ depletion [8], we also measured changes in NAD^+ levels following long-term treatment (14-days) with αSyn PFFs (68.5 nM) in SH-SY5Y-αSyn cells (Fig. 4d). To evaluate if concurrent treatment with PARPi had an effect in αSyn PFF-induced PARP-1 hyperactivation and subsequent NAD^+ depletion, SH-SY5Y-αSyn cells were treated with αSyn PFFs (68.5 nM) in the presence or absence of PARPi (**10e** (10 μM), olaparib (1 μM), or veliparib (10 μM)) for 14 days (Fig. 4d). Following treatment, we used a commercially available luminescence-based assay to measure intracellular NAD^+ levels. Based on the results from these experiments (Fig. 4d), we found that pre-treatment with **10e** notably reduced αSyn PFF-induced accumulation of both PAR and phosphorylated/high molecular weight (HMW) αSyn aggregates. Furthermore, we report that concurrent treatment with **10e** helped maintain basal NAD^+ levels and prevented αSyn PFF-induced NAD^+ depletion.

Discussion

PARP-1-mediated cell death "parthanatos" has been linked to neuronal loss in PD [11, 32] and HD [12, 32, 33], and increased PARP-1 activity has been reported in AD [34].

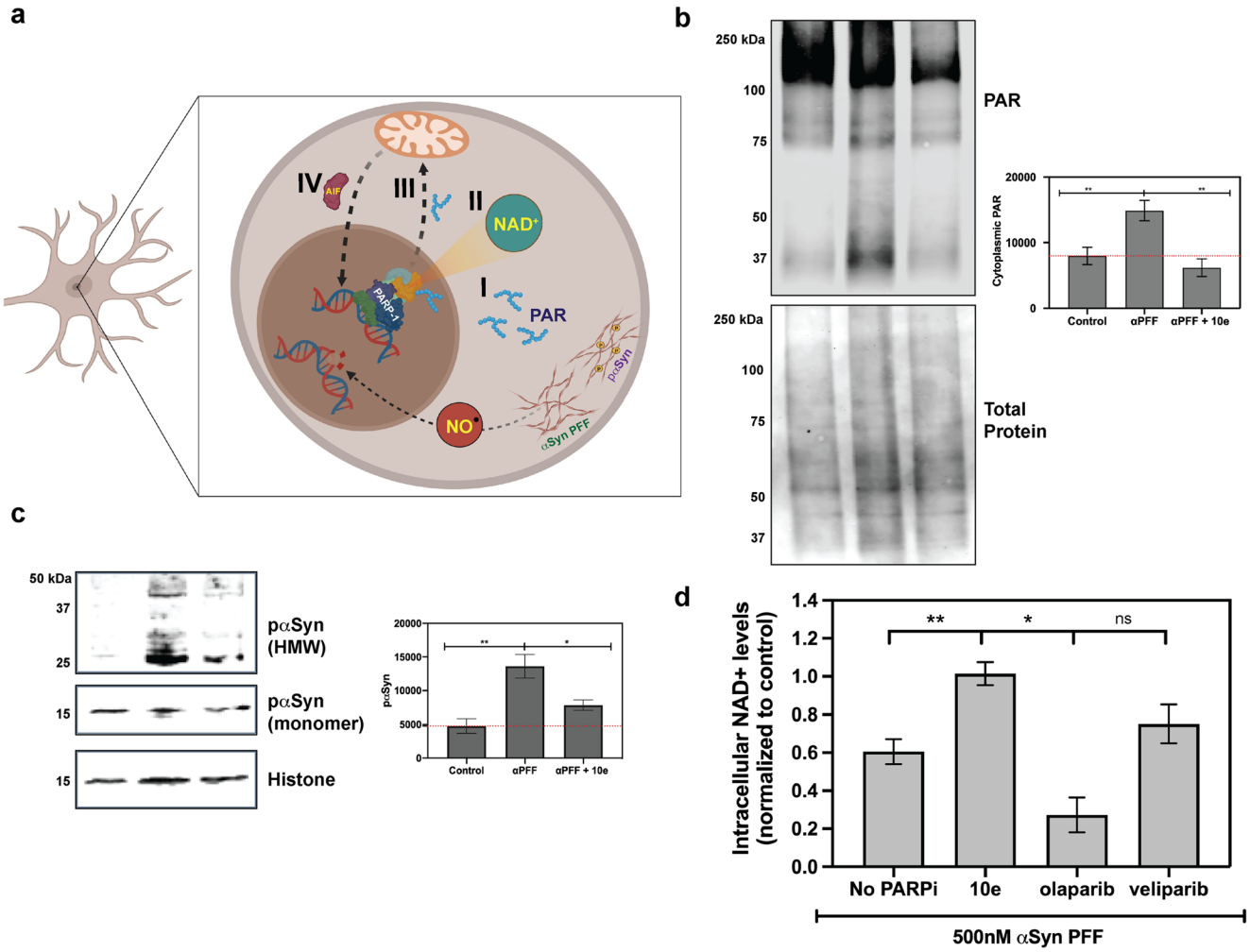

Fig. 4 (**a**) Schematic of αSyn PFF-mediated DNA damage and subsequent PARP-1 hyperactivation resulting in: (I) cytoplasmic accumulation of PAR, (II) depletion of NAD^+, (III) crosstalk between PAR and the mitochondria, and (IV) translocation of AIF from the mitochondria to the nucleus, resulting in chromatin fragmentation and cell death. (**b**) (*Top*) PAR immunoblot of cytoplasmic protein lysates from SH-SY5Y-αSyn cells 48-h post-treatment and *(from left-to-right)* untreated control, αSyn PFF-only, and αSyn PFF + **10e**. (*Bottom*) REVERT 700 total protein stain. (*Right*) Dosimetry measurements of total PAR signal intensity. Bars represent means ± SEM (n =3). $^{**}P < 0.001$. (**c**) (*Top*) Phosphorylated αSyn (pαSyn) immunoblot from SH-SY5Y-αSyn cells 48-h post-treatment *(from left to right)* untreated control, αSyn PFF-only, αSyn PFF + **10e**. (*Bottom*) Histone loading control. (*Right*) Dosimetry intensity values of HMW phosphorylated αSyn. Bars represent means ± SEM (n =3). $^{*}P < 0.01$, $^{**}P < 0.001$. (**d**) Intracellular NAD^+ levels 14-day post-αSyn PFF treatment in the presence or absence of PARPi. Luminescence values from untreated control samples were used to normalize the raw values for all treated conditions. Bars represent means ± SEM (n =3). $^{*}P < 0.01$, $^{**}P < 0.001$

Consequently, in the last decade, a number of studies have evaluated PARPi as potential treatment options for neurological disease conditions associated with PARP hyperactivation [35–37]. However, there are valid concerns about the effects of inhibiting physiological PARP activity in the brain and how inhibition of this DNA repair enzyme may affect normal DNA repair function. As a result, when repurposing and/or designing PARPi for therapeutic indications, certain criteria will need to be taken into consideration. First, investigators will need to establish a therapeutic window in animal models of neurodegeneration in order to fully validate the neuroprotective effects of these PARPi therapies—this step will be critical in ensuring the successful translation of PARPi from experimental models to patients in the clinic. In addition, since numerous studies have demonstrated that PARPi cytotoxicity in cancer and healthy cells is driven by PARP-1 trapping mechanisms [21, 31], PARPi intended for neurological applications will need to exhibit "weak trapping" characteristics in order to limit possible cellular toxicity due to toxic PARP-1-DNA interactions (PARP trapping).

In this study, we set out to evaluate the therapeutic potential of a novel low-toxicity olaparib analogue (**10e**) (Fig. 1 a and b) for applications outside of oncology. In vitro studies with **10e** in human neuronal lines revealed that the novel PARPi holds therapeutic potential in non-oncological disease settings. This is evidenced by the fact that **10e** displays

significantly lower cellular toxicity in SH-SY5Y-WT cells when compared to olaparib, veliparib, and PJ-34 (Fig. 1a). Along with **10e**, we also evaluated the toxicity profiles of other olaparib analogues (**10a**, **10b**, **12a**, **14a**, and **17a**) (Fig. 1a), originally identified by our group [22], and characterized their PARP-2 trapping properties (Fig. 1c). Our studies revealed that some of these analogues (**10b**, **12a**, and **14a**) displayed similar low-toxicity effects in SH-SY5Y-WT cells compared to **10e** (Fig. 1a); however, most of these analogues—with the exception of **14a** and **17a**—displayed notable PARP-2 trapping (Fig. 1c), thus limiting their use as PARP-1 selective compounds.

We also set out to confirm the target specificity of **10e** by performing cell toxicity studies in both IMR-5 PARP-1/WT and IMR-5 PARP-1/KO cell lines (Fig. 1d). In accordance with our previous studies [22], our results show that **10e** exhibits high PARP-1 selectivity. However, at higher doses >10μM, off-target effects were observed in the PARP-1/KO line (Fig. 1d), these effects were likely due to interactions with other PARPs (i.e., PARP-2); as a result, these potential off-target effects will need to be taken into consideration when designing future animal efficacy studies with **10e**.

Next, characterization studies showed that **10e** demonstrates neuroprotective effects against DNA damage (Fig. 2a) and oxidative stress-mediated cell death (Fig. 2b). In addition, we confirm that **10e** displays significantly lower DNA damaging properties compared to olaparib (Fig. 2c). These results are in accordance with our previous studies [22] which show significantly increased γH_2AX staining in olaparib-treated cells, when compared to **10e**-treated cells. Accordingly, we set out to explore the pharmacological properties of **10e** in order to better understand why the cellular (i.e., cell killing) effects of this compound differ from olaparib. To answer this, we performed two different PARP-1 trapping assays (biochemical and microscopy-based) to evaluate the PARP-1 trapping effects of **10e**.

In the biochemical trapping assay, the differences in trapping potency between **10e** and olaparib were evident under conditions of genotoxic stress, i.e., MMS treatment (Fig. 3 a and b). However, in order to detect differences in PARP-1 trapping potencies between inhibitors (without the need to include MMS in the samples), we increased the PARPi treatment time to 24 h and used a microscopy-based PARP-1 trapping assay (Fig. 3 c and d) to measure PARP-1 signal intensity per cell for each treatment condition. From this, we noted that **10e** displayed significantly lower PARP-1 trapping effects when compared to olaparib and similar effects compared to veliparib. Based on these results, we conclude that the differences in trapping potencies for olaparib and **10e** likely account for the disparity in cytotoxicity between the two compounds. Interestingly, based on dose-response data gathered from IMR-5 treated cells (Fig. 1b) and the microscopy-based PARP-1 trapping assay (Fig. 3 c and d), it appears that the cellular effects of **10e** are more comparable with veliparib than olaparib. On the other hand, while **10e** and veliparib share some similarities in terms of cellular effects (i.e., lower toxicity and weaker trapping properties), it is important to note that **10e** performs better than veliparib at preventing NAD^+ depletion resulting from αSyn PFF-mediated effects (Fig. 4d). Therefore, **10e** may offer better therapeutic properties for use in neurological disease applications.

In addition to "weak trapping" effects, **10e** also exhibits neuroprotective properties. Results from experiments conducted in the SH-SY5Y-αSyn cell line show that αSyn PFFs both activate PARP-1 and promote the accumulation of PAR polymer in the cytoplasm of these cells (Fig. 4b). Not surprisingly, when pre-treated with **10e**, the cytoplasmic accumulation of PAR in αSyn PFF-treated cells is notably diminished (Fig. 4b). In addition, **10e** also reduces the formation of HMW forms of phosphorylated αSyn (Fig. 4c), a form of αSyn that is associated with increased PD-like pathology. Furthermore, we report that when SH-SY5Y-αSyn cells are treated with αSyn PFFs for 14 days, these cells experience a 60% reduction in NAD^+ levels compared to untreated controls (Fig. 4d). Interestingly, when these cells are pre-treated with **10e** prior to αSyn PFF treatment, the levels of NAD^+ remain unchanged, thus suggesting that pre-treatment with **10e** protects these cells against αSyn PFF-mediated NAD^+ depletion. Additionally, due to the long-term nature of this treatment regimen (14 days), cells that were pre-treated with olaparib (1 μM) likely suffered from olaparib-mediated toxicity, as evidenced by a significant decrease in NAD^+ levels in the olaparib + αSyn PFF-treated samples compared to the αSyn PFF-only (No PARPi) samples (Fig. 4d). On the other hand, cells that were pre-treated with veliparib had slightly higher levels of NAD^+ compared to αSyn PFF-only (no PARPi) samples (Fig. 4d). Notably, the neuroprotective effects of veliparib were not as pronounced as those of **10e** (Fig. 4d). Based on this, **10e** may be a more attractive PARPi than veliparib for neuro-based therapeutic applications. Overall, these early results are encouraging and provide proof-of-concept for using this novel PARPi (**10e**) for potential therapeutic applications in non-oncological disease conditions.

Future studies will focus on validating **10e** in PD-like animal models in order to evaluate the neuroprotective effects of this compound in vivo. Altogether, the data presented in this study—along with our previously published findings [22]—provide scientific support for further evaluating **10e** as a potential therapeutic strategy for neurological disease conditions such as PD.

Methods

Cell Culture

IMR-5 cells were maintained in DMEM media with 10% heat-inactivated fetal calf serum (FBS), 100 units/mL

penicillin, and 100 μg/mL streptomycin (Pen-Strep). SH-SY5Y-WT and SH-SY5Y-αSyn cells were maintained in DMEM/F12 media with GlutaMAX supplement (Thermo Fisher Scientific, Cat# 10565018), 10% FBS, and 100 μg/mL Pen-Strep. Cells were maintained in a humid atmosphere of 5% CO_2 and 95% O_2 at 37 °C.

Cell Viability Assays

IMR-5 cells were seeded in black wall, clear bottom 96-well plates (Corning®) at concentrations of 1000 cells/well and were treated with varying concentrations of PARPi for 7 days to establish a dose-response curve. Similarly, SH-SY5Y-WT cells were seeded at concentrations of 2000 cells/well and treated with 10 μM PARPi or PBS (control) for 7 days. Following treatment incubation, the cells were assayed for viability using the luminescent-based assay, CellTiter Glo (Promega Corp.), following manufacturer's protocol. Plates were read on an EnSpire multimode plate reader (PerkinElmer, Inc.). Data was normalized to percent (%) survival at each concentration and evaluated by dividing the luminescent signal in treated wells by the average of PBS controls. Experiments were repeated three times.

Drug Preparation

Olaparib and veliparib were obtained from Selleckchem (Cat# S1060 and Cat# S1004, respectively). PJ-34 was purchased from Tocris (Cat# 3255). Drug stock solutions were made in DMSO at 20 mM. The stock solutions were stored at −20°C in the dark and diluted in culture medium immediately before use. Methyl methanesulfonate (MMS) was prepared fresh each time from 9 M stock (Sigma-Aldrich, Cat# 129925) in PBS and then diluted in culture medium to final concentration.

Generation of IMR-5 PARP-1/KO Line

IMR-5 PARP-1 knockouts were generated using a two-vector *Streptococcus pyogenes* (Sp) Cas9 system. sgRNAs were designed to target the functional domain of the protein and were cloned by annealing the two complementary DNA oligos into a BsmB1-digested vector using T4 DNA ligase as described in [38].

Immunofluorescence

SH-SY5Y-WT cells were seeded at a concentration of 20,000 cells/well (Lab-Tek II Chamber Slide, 8 well, Cat# 154941) for 48 h. Cells were then treated with a 10 μM dose of PARPi for 24 h. Following treatment, cells were washed in ice-cold PBS, fixed in 4% paraformaldehyde, washed 3X with PBS, and permeabilized with 0.1% Triton X-100 for 10 min at RT. After permeabilization, the cells were washed 3X with PBS-T (PBS with 0.1% Tween-20) at RT. After the third wash, 200 μL of 10% goat serum (Thermo Fisher, Cat# 50062Z) was added to each well for 1 h at RT to block non-specific immuno binding. After blocking, the cells were incubated with primary antibodies targeting RAD51 (abcam, ab63801, 1:200) for 1 h at 37°C. The cells were then incubated with secondary antibody (Invitrogen, Cat# A32731, Alexa Fluor™ Plus 488, 1:200) for 1 h at 37°C, washed 3X with PBS-T, and mounted with ProLong™ Glass Antifade w/NucBlue (Invitrogen, Cat # P36985). Coverslips were placed on each slide and the slides were allowed to dry overnight at 4°C. Images were captured using Zeiss Axio Widefield (20x/0.8) microscope.

Fluorescence-Based PARP-1/2 Trapping

SH-SY5Y-WT cells were seeded at a concentration of 16,000 cells/well (Lab-Tek II Chamber Slide, 8 well, Cat# 154941) for 48 h. Cells were then treated with a 10 μM dose of PARPi for 24 h. Following treatment, cells were washed in ice-cold PBS, and non-chromatin-bound proteins were solubilized in a 2% solution of Triton-X detergent in PBS for 2 min; the cells were then fixed in 4% paraformaldehyde, washed 3X with PBS, and permeabilized with 0.1% Triton X-100 for 10 min at RT. After permeabilization, the cells were washed 3X with PBS-T (PBS with 0.1% Tween-20) at RT. After the third wash, 200 μL of 10% goat serum (Thermo Fisher, Cat# 50062Z) was added to each well for 1 h at RT to block non-specific immuno binding. After blocking, the cells were incubated with primary antibodies targeting either PARP-1 (Cell Signaling Technology, 46D11, 1:1,000) or PARP-2 (Active Motif, Cat# 39742, 1:200) overnight at 4°C. Following primary antibody incubation, the cells were washed 3X with PBS-T. After the third wash, the cells were then incubated with secondary antibody (Invitrogen, Cat# A32731, Alexa Fluor™ Plus 488, 1:400) for 1 h at RT, washed 3X with PBS-T, and mounted with ProLong™ Glass Antifade w/NucBlue (Invitrogen, Cat # P36985). Coverslips were placed on each slide, and the slides were allowed to dry overnight at 4°C. Images were captured using Zeiss Axio Widefield (20x/0.8) microscope.

Biochemical PARP-1 Trapping

Following treatment incubation, the cell samples were processed according to the manufacturer's protocol (Thermo Scientific Subcellular Protein Fractionation Kit for Cultured Cells, Cat# 78840) in order to obtain subcellular protein fractions and isolate chromatin-bound proteins. The resulting chromatin extracts were then directly processed for downstream immunoblotting of PARP-1 (Cell Signaling Technology, Cat# 9532S, PARP 46D11 1:1,000).

αSyn Protein Expression and Purification

Protein expression and purification was done following previously published protocol [39]. Briefly, the plasmid encoding the human αSyn sequence was transformed into *Escherichia coli* BL21(DE3), and the cells were grown on agar/LB plates with ampicillin (100 μg/mL) overnight at 37°C. The next day, a single colony was inoculated into 100 mL Luria-Bertani (LB) containing ampicillin (100 μg/mL). The culture was incubated at 37°C overnight with shaking at ~200 rpm. The following day, 10 mL of the overnight culture was diluted with 1 L of LB media supplemented with ampicillin, and this culture was incubated at 37°C until OD_{600} reached 0.6–0.7. Protein expression was induced by addition of isopropyl-β-D-thiogalactoside (IPTG) to a final concentration of 1 mM and continued to grow at 18°C overnight. After induction, cells were harvested by centrifugation at 4°C (20 min, 4000*g*). The typical yield of wet-cell paste was 2 g/L. Cells were suspended in a lysis buffer (5 mL for 1 g of cell paste) containing 25 mM Tris, 20 mM imidazole, 50 mM NaCl (pH 8) with a protease inhibitor (phenylmethylsulfonylfluoride, 0.5 mM final concentration and protease inhibitor cocktail from Cell Signaling Technology). Cells were lysed by sonication on ice for 10 min (20 s on, 20 s off). The crude cell lysate was then centrifuged at 20,000*g* for 30 min, and the supernatant was mixed with Ni-NTA resin (Clontech, 3 mL) and kept on a rocker at RT for 30 min. The resin was then washed with 100 mL wash buffer (25 mM Tris, 20 mM imidazole, 50 mM NaCl, pH 8). The protein was eluted with a buffer containing 25 mM Tris, 300 mM imidazole, and 50 mM NaCl (pH 8). Fractions containing the protein were identified by UV-Vis spectroscopy and combined and was treated with β-mercaptoethanol (200 mM final concentration) overnight at RT to cleave the C-terminal linker. The next day, the protein was concentrated to 3 mL and dialyzed against 1X PBS buffer. After dialysis, the protein mixture was loaded onto Ni-NTA column, and the pure αSyn protein was collected in the flow through fractions. The combined protein fractions were concentrated and dialyzed against 1X PBS buffer. The purity of the protein was confirmed by SDS-PAGE. Protein concentration was determined by measuring the absorbance at 280 nm and using the calculated (ExPASy) extinction coefficient of 5960 $M^{-1}cm^{-1}$.

Preparation of αSyn Pre-formed Fibrils

Purified αSyn monomer (100 μM) was incubated in 1X PBS for 7 days at 37 °C with shaking at 1000 rpm in an Eppendorf ThermoMixer F1.5.

Immunoblotting

For pαSyn immunoblotting (abcam, Cat# ab51253, 1:1,000), cells were gently washed twice with ice-cold PBS and scraped into ice-cold buffer (TBS, 50 mM Tris-HCL pH 7.4, 175 mM NaCl, and 5 mM EDTA)) containing 1X protease and phosphatase inhibitors (Thermo Scientific, Halt™ Protease and Phosphatase Inhibitor Cocktail), lysed using a probe sonicator (Fisher Scientific, CL-18 probe), and the lysates were ultracentrifuged for 20 min at 100,000*g* at 4°C. The pellet was washed twice, resuspended in TBS buffer with 1% Triton X-100, sonicated, and centrifuged for 20 min at 100,000*g* at 4°C. The supernatant was collected, and protein was quantified using BioRad DC protein quantification assay, following manufacturer's protocol. For PAR immunoblotting (Cell Signaling Technology, Cat# E6F6A, 1:1,000), samples were processed for subcellular fractionation following manufacturer's protocol (Thermo Scientific Subcellular Protein Fractionation Kit for Cultured Cells, Cat# 78840). Cytoplasmic protein fractions were then processed for downstream immunoblotting. All immunoblot samples were diluted to a final concentration of 2 μg/μL with 1X Laemmli buffer. Samples were separated on 4–20% BioRad TGX pre-packed gels at 100 V for 1 h. Gels were transferred to a PVDF membrane using BioRad turbo transfer at 1.3 A for 5 min. Next, membranes were washed 4X in PBS with 0.2% Tween-20 and incubated in Odyssey Blocking buffer (Li-COR), 0.2% Tween-20, and 0.1% SDS for 1 h. Membranes were incubated overnight at 4°C with primary antibodies and detected with fluorescent secondary antibodies (Invitrogen, Alexa Fluor™ Plus 680 Goat anti-Mouse (PAR) or Alexa Fluor™ Plus 800 Goat anti-Rabbit (pαSyn)). Uniform regions of interest were applied to each lane to calculate total fluorescence intensity. Either Histone H3 *loading control* (Cell Signaling Technology, Cat# 96C10) or Revert 700 stain *total protein* (Li-COR, Revert 700 Total Protein, Cat# 926-11011) were used to calculate final relative protein expression for each lysate. Following Revert 700 stain, membranes were washed 2X with Revert 700 wash buffer (Li-COR) for 5 min each. Membranes were imaged using Li-COR ODYSSEY CLx scanner.

NAD-Glo™ Assay

A commercially available NAD^+ detection assay (Promega, NAD/NADH-Glo™, Cat# G9071) was used for measurements of cellular NAD^+ levels from treated cell samples. Briefly, SH-SY5Y-αSyn cells were seeded in white luminometer 96-well plates (Greiner bio-one, Cat# 655083) at a concentration of 1000 cells/well for 24 h. Cells were then treated with αSyn PFFs (500 nM), in the presence or absence of PARPi, for 14 days. Cell media with or without PARPi were replenished on day 7 to prevent media evaporation and maintain drug stability. Following 14-day treatment, cells were gently washed with 1X PBS and resuspended in 50 μL of PBS per well. Samples were then lysed by adding 50 μL of base solution (0.2 N NaOH) with 1% DTAM (Sigma Cat# D8638). Following cell lysis, samples were split into two

new wells, one well was treated with acid (0.4 N HCL) to measure NAD^+ levels, and the second sample was treated with base solution (0.2 N NaOH) to measure NADH levels. Both samples were then heated for 15 min at 60°C. Acid-treated samples were then treated with 25 μL of 0.5 M Trizma base solution (Sigma-Aldrich, Cat# T6791-100G), while base-treated samples were treated with 50 μL of HCL/Trizma solution. Following sample preparation, NAD^+/NADH levels were measured following manufacturer's protocol.

Quantification and Statistical Analysis

All measurements were taken from distinct samples. Data points in each graph are mean (± SEM), where "n" indicates the number of biological replicates for each experiment. *T*-tests and one-way and two-way ANOVAs were performed and are described in each figure legend. Statistical significance was set at $P < 0.05$. All statistical analyses were carried out using GraphPad Prism 8 software.

Abbreviations PARP-1, Poly(ADP-ribose) polymerase-1; PARPi, PARP inhibitor; PD, Parkinson's disease; αSyn, Alpha-synuclein; PFF, Pre-formed fibrils; PAR, Poly (ADP-ribose); NAD^+, Nicotinamide adenine dinucleotide

Acknowledgements SH-SY5Y-WT and SH-SY5Y-αSyn cells were a gift from Dr. Harry Ischiropoulos, University of Pennsylvania. IMR-5 cells were a gift from Dr. John Maris, University of Pennsylvania. The plasmid encoding the human αSyn sequence was a gift from Dr. James Petersson, University of Pennsylvania.

Author Contribution L.N.P. designed the experiments presented in this study and performed all the cell/biochemical and microscopy-based experiments. Z.L.Z. helped produce all the purified proteins and fibrils used in this project. L.N.P. and Z.L.Z. prepared the manuscript. S.W.R. synthesized **10e** and the other olaparib analogues described in this manuscript. Z.L.Z. and R.H.M provided support with experimental design.

Funding This research was supported by the Michael J. Fox Foundation (R.H.M.) and U19-NS110456 (R.H.M.) and supported in part by T32GM008076 (L.N.P.).

Data and Materials Availability All data generated and analyzed in this study are included in this published article.

Declarations

Consent to Participate/Consent for Publication Not applicable.

Conflict of Interest The authors declare no competing interests.

References

1. Deshmukh D, Qiu Y (2015) Role of PARP-1 in prostate cancer. Am J Clin Exp Urol 3(1):1–12
2. Ba X, Garg NJ (2011) Signaling mechanism of poly(ADP-ribose) polymerase-1 (PARP-1) in inflammatory diseases. Am J Pathol 178(3):946–955
3. Rosado MM, Bennici E, Novelli F, Pioli C (2013) Beyond DNA repair, the immunological role of PARP-1 and its siblings. Immunology 139(4):428–437
4. Wei W, Li Y, Lv S, Zhang C, Tian Y (2016) PARP-1 may be involved in angiogenesis in epithelial ovarian cancer. Oncol Lett 12(6):4561–4567
5. Malapetsa A, Noe AJ, Poirier GG, Desnoyers S, Berger NA, Panasci LC (1996) Identification of a 116 kDa protein able to bind 1,3-bis(2-chloroethyl)-1-nitrosourea-damaged DNA as poly(ADP-ribose) polymerase. Mutat Res 362(1):41–50
6. Ray Chaudhuri A, Nussenzweig A (2017) The multifaceted roles of PARP1 in DNA repair and chromatin remodelling. Nat Rev Mol Cell Biol 18(10):610–621
7. Hassa PO, Haenni SS, Elser M, Hottiger MO (2006) Nuclear ADP-ribosylation reactions in mammalian cells: where are we today and where are we going? Microbiol Mol Biol Rev 70(3):789–829
8. David KK, Andrabi SA, Dawson TM, Dawson VL (2009) Parthanatos, a messenger of death. Front Biosci (Landmark edition) 14:1116
9. McGurk L, Mojsilovic-Petrovic J, Van Deerlin VM, Shorter J, Kalb RG, Lee VM, Trojanowski JQ, Lee EB et al (2018) Nuclear poly(ADP-ribose) activity is a therapeutic target in amyotrophic lateral sclerosis. Acta Neuropathol Commun 6(1):84
10. Strosznajder JB, Czapski GA, Adamczyk A, Strosznajder RP (2012) Poly(ADP-ribose) polymerase-1 in amyloid beta toxicity and Alzheimer's disease. Mol Neurobiol 46(1):78–84
11. Kam T-I, Mao X, Park H, Chou S-C, Karuppagounder SS, Umanah GE, Yun SP, Brahmachari S et al (2018) Poly(ADP-ribose) drives pathologic α-synuclein neurodegeneration in Parkinson's disease. Science 362(6414):eaat8407
12. Liu C, Fang Y (2019) New insights of poly(ADP-ribosylation) in neurodegenerative diseases: a focus on protein phase separation and pathologic aggregation. Biochem Pharmacol 167:58–63
13. Anderson JP, Walker DE, Goldstein JM, de Laat R, Banducci K, Caccavello RJ, Barbour R, Huang J et al (2006) Phosphorylation of Ser-129 is the dominant pathological modification of α-synuclein in familial and sporadic Lewy body disease. J Biol Chem 281(40): 29739–29752
14. McGurk L, Gomes E, Guo L, Mojsilovic-Petrovic J, Tran V, Kalb RG, Shorter J, Bonini NM (2018) Poly(ADP-Ribose) prevents pathological phase separation of TDP-43 by promoting liquid demixing and stress granule localization. Mol Cell 71(5):703–717 e709
15. McGurk L, Gomes E, Guo L, Shorter J, Bonini NM (2018) Poly(ADP-ribose) engages the TDP-43 nuclear-localization sequence to regulate granulo-filamentous aggregation. Biochemistry 57(51):6923–6926
16. Outeiro TF, Grammatopoulos TN, Altmann S, Amore A, Standaert DG, Hyman BT, Kazantsev AG (2007) Pharmacological inhibition of PARP-1 reduces alpha-synuclein- and MPP+-induced cytotoxicity in Parkinson's disease in vitro models. Biochem Biophys Res Commun 357(3):596–602
17. McCann KE (2019) Advances in the use of PARP inhibitors for BRCA1/2-associated breast cancer: talazoparib. Future Oncol 15(15):1707–1715
18. Syed YY (2017) Rucaparib: first global approval. Drugs 77(5): 585–592
19. Scott LJ (2017) Niraparib: first global approval. Drugs 77(9):1029–1034
20. Kim G, Ison G, McKee AE, Zhang H, Tang S, Gwise T, Sridhara R, Lee E et al (2015) FDA approval summary: olaparib monotherapy in patients with deleterious germline BRCA-mutated advanced

ovarian cancer treated with three or more lines of chemotherapy. Clin Cancer Res 21(19):4257–4261
21. Zandarashvili L, Langelier M-F, Velagapudi UK, Hancock MA, Steffen JD, Billur R, Hannan ZM, Wicks AJ et al (2020) Structural basis for allosteric PARP-1 retention on DNA breaks. Science 368(6486):eaax6367
22. Reilly SW, Puentes LN, Wilson K, Hsieh C-J, Weng C-C, Makvandi M, Mach RH (2018) Examination of diazaspiro cores as piperazine bioisosteres in the olaparib framework shows reduced DNA damage and cytotoxicity. J Med Chem 61(12):5367–5379
23. Abdelkarim GE, Gertz K, Harms C, Katchanov J, Dirnagl U, Szabo C, Endres M (2001) Protective effects of PJ34, a novel, potent inhibitor of poly(ADP-ribose) polymerase (PARP) in in vitro and in vivo models of stroke. Int J Mol Med 7:255–260
24. Loibl S, O'Shaughnessy J, Untch M, Sikov WM, Rugo HS, McKee MD, Huober J, Golshan M et al (2018) Addition of the PARP inhibitor veliparib plus carboplatin or carboplatin alone to standard neoadjuvant chemotherapy in triple-negative breast cancer (BrighTNess): a randomised, phase 3 trial. Lancet Oncol 19(4): 497–509
25. Faro R, Toyoda Y, McCully JD, Jagtap P, Szabo E, Virag L, Bianchi C, Levitsky S et al (2002) Myocardial protection by PJ34, a novel potent poly (ADP-ribose) synthetase inhibitor. Ann Thorac Surg 73(2):575–581
26. Dasgupta A, Shields JE, Spencer HT (2012) Treatment of a solid tumor using engineered drug-resistant immunocompetent cells and cytotoxic chemotherapy. Hum Gene Ther 23(7):711–721
27. Michelena J, Lezaja A, Teloni F, Schmid T, Imhof R, Altmeyer M (2018) Analysis of PARP inhibitor toxicity by multidimensional fluorescence microscopy reveals mechanisms of sensitivity and resistance. Nat Commun 9(1):2678. https://doi.org/10.1038/s41467-018-05031-9
28. Shi J, Wang E, Milazzo JP, Wang Z, Kinney JB, Vakoc CR (2015) Discovery of cancer drug targets by CRISPR-Cas9 screening of protein domains. Nat Biotechnol 33(6):661–667
29. Sharma A, Singh K, Almasan A (2012) Histone H2AX phosphorylation: a marker for DNA damage. In: Bjergbæk L (ed) DNA repair protocols. Humana Press, Totowa, NJ, pp. 613–626
30. Mladenov E, Anachkova B, Tsaneva I (2006) Sub-nuclear localization of Rad51 in response to DNA damage. Genes Cells 11(5): 513–524
31. Hopkins TA, Shi Y, Rodriguez LE, Solomon LR, Donawho CK, DiGiammarino EL, Panchal SC, Wilsbacher JL et al (2015) Mechanistic dissection of PARP1 trapping and the impact on in vivo tolerability and efficacy of PARP inhibitors. Mol Cancer Res 13(11):1465–1477
32. Narne P, Pandey V, Simhadri PK, Phanithi PB (2017) Poly(ADP-ribose)polymerase-1 hyperactivation in neurodegenerative diseases: the death knell tolls for neurons. Semin Cell Dev Biol 63: 154–166
33. Cardinale A, Paldino E, Giampà C, Bernardi G, Fusco FR (2015) PARP-1 inhibition is neuroprotective in the R6/2 mouse model of Huntington's disease. PLoS One 10(8):e0134482
34. Love S, Barber R, Wilcock G (1999) Increased poly (ADP-ribosyl) ation of nuclear proteins in Alzheimer's disease. Brain 122(2):247–253
35. Mandir AS, Przedborski S, Jackson-Lewis V, Wang ZQ, Simbulan-Rosenthal CM, Smulson ME, Hoffman BE, Guastella DB et al (1999) Poly(ADP-ribose) polymerase activation mediates 1-methyl-4-phenyl-1, 2,3,6-tetrahydropyridine (MPTP)-induced parkinsonism. Proc Natl Acad Sci U S A 96(10):5774–5779
36. Martire S, Mosca L, d'Erme M (2015) PARP-1 involvement in neurodegeneration: a focus on Alzheimer's and Parkinson's diseases. Mech Ageing Dev 146-148:53–64
37. Wang H, Shimoji M, Yu SW, Dawson TM, Dawson VL (2003) Apoptosis inducing factor and PARP-mediated injury in the MPTP mouse model of Parkinson's disease. Ann N Y Acad Sci 991:132–139
38. Verma P, Zhou Y, Cao Z, Deraska PV, Deb M, Arai E, Li W, Shao Y et al (2021) ALC1 links chromatin accessibility to PARP inhibitor response in homologous recombination-deficient cells. Nat Cell Biol 23(2):160–171
39. Lengyel-Zhand Z, Ferrie JJ, Janssen B, Hsieh C-J, Graham T, Xu K-y, Haney CM, Lee VMY, Trojanowski JQ, Petersson EJ, Mach RH (2020) Synthesis and characterization of high affinity fluorogenic α-synuclein probes. Chem Commun.